JACS
JOURNAL OF THE AMERICAN CHEMICAL SOCIETY
Article
pubs.acs.org/JACS

# Mechanical Properties of Nanoscopic Lipid Domains

Jonathan D. Nickels,[*,†,‡,⊥] Xiaolin Cheng,[§,∥] Barmak Mostofian,[§] Christopher Stanley,[†] Benjamin Lindner,[§] Frederick A. Heberle,[†,⊥] Stefania Perticaroli,[†,⊥] Mikhail Feygenson,[†] Takeshi Egami,[⊥] Robert F. Standaert,[†,∥] Jeremy C. Smith,[§,∥] Dean A. A. Myles,[†] Michael Ohl,[#] and John Katsaras[*,†,‡,⊥]

[†]Oak Ridge National Laboratory, Oak Ridge, Tennessee 37831, United States
[‡]Department of Physics and Astronomy, University of Tennessee, Knoxville, Tennessee 37996, United States
[§]Center for Molecular Biophysics, Oak Ridge National Laboratory, Oak Ridge, Tennessee 37831, United States
[∥]Department of Biochemistry and Cellular and Molecular Biology, University of Tennessee, Knoxville, Tennessee 37996, United States
[⊥]Joint Institute for Neutron Sciences, Oak Ridge, Tennessee 37831, United States
[#]Jülich Center for Neutron Science, Oak Ridge, Tennessee 37831, United States

Supporting Information

**ABSTRACT:** The lipid raft hypothesis presents insights into how the cell membrane organizes proteins and lipids to accomplish its many vital functions. Yet basic questions remain about the physical mechanisms that lead to the formation, stability, and size of lipid rafts. As a result, much interest has been generated in the study of systems that contain similar lateral heterogeneities, or domains. In the current work we present an experimental approach that is capable of isolating the bending moduli of lipid domains. This is accomplished using neutron scattering and its unique sensitivity to the isotopes of hydrogen. Combining contrast matching approaches with inelastic neutron scattering, we isolate the bending modulus of ∼13 nm diameter domains residing in 60 nm unilamellar vesicles, whose lipid composition mimics the mammalian plasma membrane outer leaflet. Importantly, the bending modulus of the nanoscopic domains differs from the modulus of the continuous phase surrounding them. From additional structural measurements and all-atom simulations, we also determine that nanoscopic domains are in-register across the bilayer leaflets. Taken together, these results inform a number of theoretical models of domain/raft formation and highlight the fact that mismatches in bending modulus must be accounted for when explaining the emergence of lateral heterogeneities in lipid systems and biological membranes.

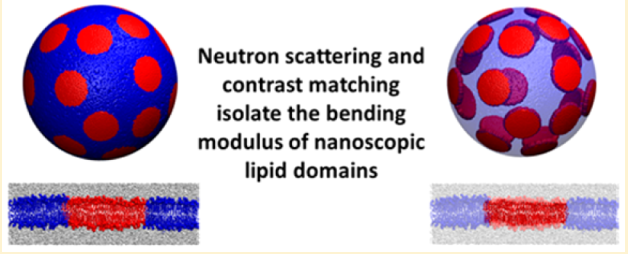


## INTRODUCTION

The existence and role of lateral lipid organization in biological membranes has been studied and contested for more than 30 years.[1] At the core of this debate is the lipid raft hypothesis,[2] which proposes rafts as scalable compartments in biological membranes, providing appropriate physical environments to resident membrane proteins. This implies that lateral lipid organization is connected to a range of biological functions, such as protein colocalization, membrane trafficking, and cell signaling, to name a few.[1a,f,2,3] Lipid rafts have even been implicated in the pathogenesis of viral and bacterial infection.[4] These roles all stem from the premise that membranes are inherently heterogeneous structures that self-organize into nanoscopic heterogeneities, or "rafts", within a "sea" of disordered lipids based on the thermodynamic and structural properties of their constituent lipids and proteins. However, fundamental questions remain about the physical mechanisms that govern the formation, size, and stability of these lateral heterogeneities.

If one accepts the premise that nanoscopic lipid heterogeneities (or nanodomains) exist at equilibrium, one must also accept that boundary energy would in general favor a reduction of interfacial length, domain coalescence, and complete phase separation. How then does one explain the presence of nanoscopic lipid heterogeneities? In vivo, active processes may prevent equilibrium from emerging, preventing the coalescence of transient compositional fluctuations by mechanisms such as protein/cytoskeletal interactions[5] or rapid lipid turnover.[6] However, nanometer sized lipid domains have been observed in model systems in which there are no active processes.[7] In the absence of active mechanisms, competing interactions are needed to offset the boundary energy resulting in modulated phase behavior.[8] A number of detailed models have been put forward exploring potential mechanisms such as mismatches in spontaneous curvature, bending modulus, membrane thickness, and interfacial stabilization.[9] These models highlight the range

Received: August 21, 2015
Published: September 28, 2015



DOI: 10.1021/jacs.5b08894
J. Am. Chem. Soc. 2015, 137, 15772−15780

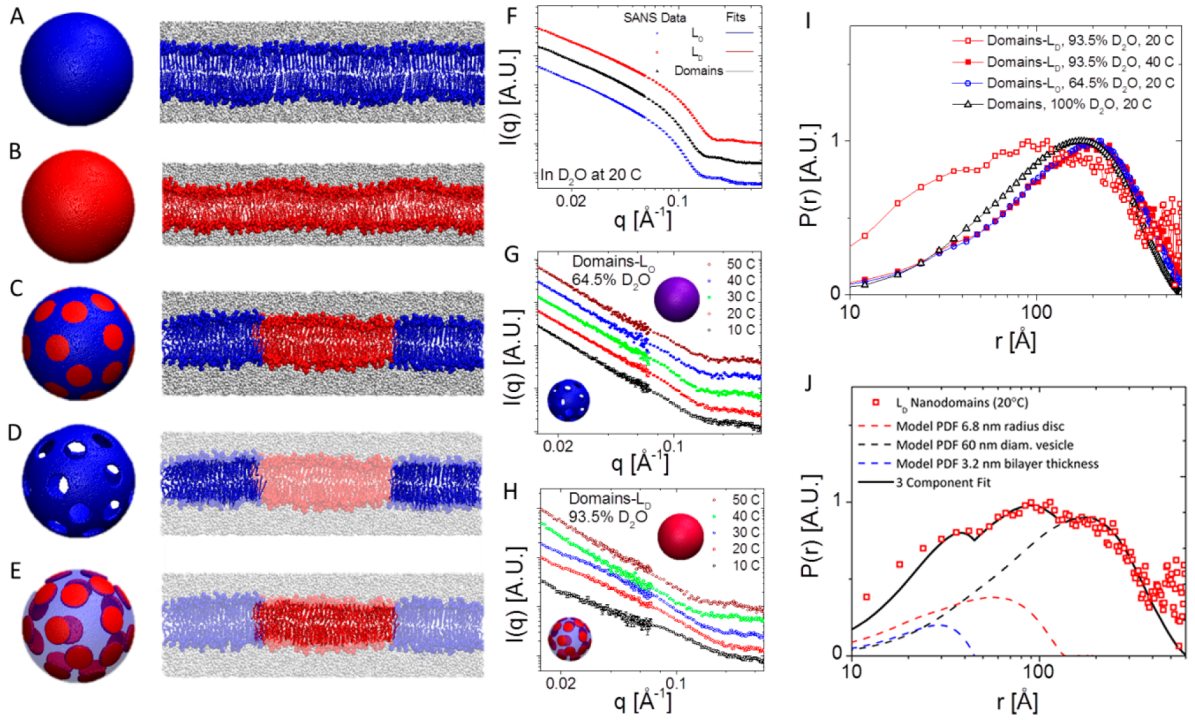


**Figure 1.** . SANS data and neutron contrast matching schemes used. Transparent coloration indicates regions of the bilayer that were contrast matched to the solvent, making them "invisible" to neutrons. (A) $L_O$, (B) $L_D$, (C) nanodomain containing composition, noncontrast matched, "Domains" (D) domain containing composition, contrast matched to emphasize the $L_O$ surround, "Domains-$L_O$", and (E) domain containing composition, contrast matched to emphasize the $L_D$ nanodomains "Domains-$L_D$" (all defined in Table S1). In this figure blue represents the $L_O$ phase; and red the $L_D$ phase. (F) SANS data and fits of the data from samples (A–C). (G) SANS data from sample D as a function of temperature. (H) SANS data from samples E as a function of temperature. (I) PDFs calculated from the SANS data emphasizing the structural changes in the Domains-$L_D$ (nanodomains) sample above and below the domain miscibility temperature of 40 °C. (J) PDF of the Domains-$L_D$ (nanodomains) sample at 20 °C compared to a model PDF, representing nanodomains that are 3.2 nm thick and of radius 6.8 nm, populating a 60 nm diameter sphere. (error bars are $\pm 2\sigma$).

of competing interactions suspected of influencing lipid phase behavior.

Given the diversity and complexity of biological membranes, simplified systems comprised of a smaller number of representative lipids are a powerful tool[7c] for understanding the phase behavior[7a] and mechanical properties[10] that may be relevant in the formation and stabilization of lipid rafts. Importantly, from the perspective of the lipid raft hypothesis, certain model mixtures exhibit liquid–liquid phase coexistence forming two phases, the liquid ordered phase ($L_O$), which is enriched in high melting lipids and cholesterol and thought to be similar to the composition of rafts, and the liquid disordered ($L_D$) phase that is thought to surrounds rafts.[11] Furthermore, some of these systems contain nanoscopic lipid heterogeneities,[7a−c] believed to be either distinct $L_D/L_O$ phases, or a single modulated phase with local compositional fluctuations. These nanoscopic heterogeneities are comparable in size to what is suggested for lipid rafts. Unfortunately, due to their nanoscopic size and compositional similarity with the surrounding lipids, as well as the potentially perturbing effects of some molecular probes, current experimental techniques provide limited information about these intriguing systems.

In the present study, we use neutron scattering and neutron scattering length density (NSLD) contrast matching techniques to observe the structure and dynamics of nanoscopic lipid heterogeneities. In brief, NSLD contrast matching is made possible because neutrons scatter differently from hydrogen ($^1$H) and deuterium ($^2$H or 'D') nuclei. Through careful isotopic substitution of the lipids and solvent, this sensitivity manifests itself in different NSLDs for the different lipid phases. This also has the advantage that isotopic substitutions are minimally perturbing to the system in other ways. Using lipid compositions obtained from published phase diagrams,[7b,12] we performed neutron scattering measurements on bilayer systems in which the NSLD of one phase matches the NSLD of the solvent. In doing so, neutrons only "see" the nonmatched phase, enabling direct measurements of the nanoscopic lipid heterogeneities populating 60 nm diameter unilamellar lipid vesicles (ULVs) (Figure 1A–E). In a novel experimental approach, we then combined this capability with inelastic neutron scattering in order to unambiguously determine the mechanical properties of the nanoscopic lipid heterogeneities populating the ULVs.

Our data reveal that the bending modulus of nanoscopic domains differs from the bending modulus of the surrounding lipid environment. Furthermore, the domains are aligned across the two leaflets of the symmetric bilayer. The composition, structure, and bending modulus of the nanoscopic heterogeneities was found to be similar to the equivalent "pure phases" predicted from the phase diagram.[7b,12] Moreover, atomistic MD simulations present a picture consistent with experimental studies, showing that domains have different structural and mechanical properties than their surrounding enviornment. The simulations also imply preferential lipid orientation at the domain interface, suggesting some degree of interfacial stabilization, akin to line activity.



DOI: 10.1021/jacs.5b08894
J. Am. Chem. Soc. 2015, 137, 15772–15780

Table 1. Summary of Structural Parameters from Neutron Experiments (20 °C) and MD Simulation ($\pm 2\sigma$)

| | $L_D$ | $L_O$ | domains (avg.) | domains $L_D$ | domains $L_O$ |
|---|---|---|---|---|---|
| thickness [Å] (SANS) | 43.9 ± 1.4 | 53.1 ± 1.0 | 51.3 ± 1.1 | | |
| avg. thickness [Å] (sim.) | 45.9 ± 0.5 | 54.2 ± 0.2 | 51.6 ± 0.6 | 46.6 ± 0.5 | 53.5 ± 0.9 |
| acyl thickness [Å] (SANS) | | | | 32.9 ± 1.8 | 38.3 ± 2.1 |
| avg. acyl thickness [Å] (sim.) | 32.6 ± 0.5 | 42.0 ± 0.2 | 39.3 ± 0.6 | 34.4 ± 0.4 | 41.2 ± 0.9 |
| area per lipid [Å$^2$] (sim.) | 54.7 ± 0.8 | 40.9 ± 0.2 | 44.5 ± 0.8 | | |
| $S_{CH}$ POPC (sim.) | 0.19 ± 0.07 | 0.32 ± 0.10 | 0.26 ± 0.08 | | |
| $S_{CH}$ DSPC (sim.) | 0.22 ± 0.07 | 0.38 ± 0.10 | 0.35 ± 0.09 | | |
| $K$ [$k_BT$] (NSE) | 17.3 ± 3.2 | 196.0 ± 42.5 | 126.5 ± 29.9 | 18.4 ± 9.8 | |
| $K$ [$k_BT$] (sim.) | 19.1 ± 1.4 | 61.8 ± 2.2 | 52.5 ± 2.3 | 18.0 ± 1.7 | |

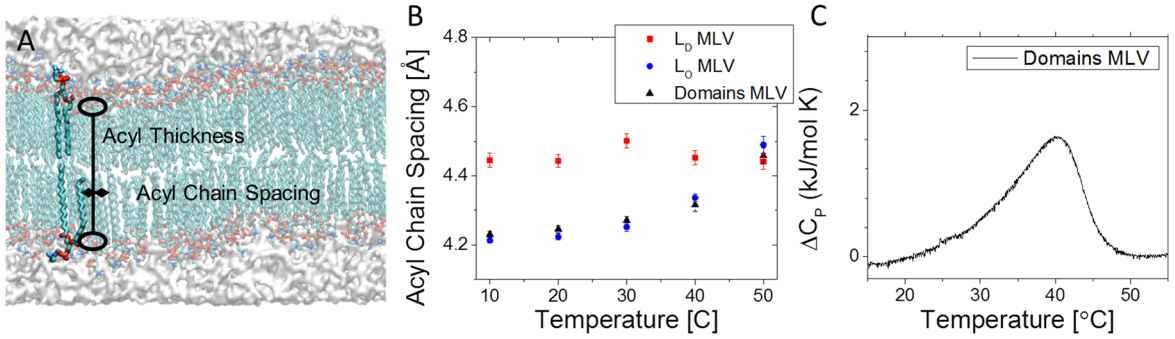


**Figure 2.** (A) Graphical representation of the acyl chain parameters calculated from SANS and ND data. (B) Acyl chain spacings from neutron diffraction measurements. (C) DSC shows a broad transition centered at ~40 °C in MLVs of the "Domains" sample, indicating domain mixing with the surround. These data are in agreement with structural changes at 40 °C in Figure 1H,I. (error bars are $\pm 2\sigma$).

## RESULTS

**Making Domains "Visible".** Nanoscopic lipid heterogeneities have been studied in model systems with as few as three components: cholesterol, one high- and one low-melting temperature lipid.[13] The four component system composed of cholesterol (Chol), 1,2-distearoyl-*sn*-glycero-3-phosphocholine (DSPC), 1-palmitoyl-2-oleoyl-*sn*-glycero-3-phosphocholine (POPC), and 1,2-dioleoyl-*sn*-glycero-3-phosphocholine (DOPC) enables one to tune domain size, from microscopic to nanoscopic dimensions, simply by varying the ratio of the two low-melting temperature lipids.[7b,12] In this study, we focus on nanoscopic domains of radius 5−7 nm formed by a mixture of Chol., DSPC, and POPC in a 22:39:39 ratio.[7b,12,14]

The compositions of the coexisting $L_D$ and $L_O$ phases (Table S1) are obtained from the ternary phase diagram,[7b,12,14,15] and their relative abundance in the nanodomain containing sample is obtained from the tie line. Based on this, we are able to tune the NSLD of each phase through judicious hydrogen/deuterium substitution of the constituent lipids. By also varying the $D_2O/H_2O$ ratio of the aqueous solvent, we can match the NSLD of one phase to that of the solvent, rendering it effectively "invisible" to neutrons. This enables neutron techniques to isolate the scattering from only the noncontrast matched phase (Figure 1A−E, Tables S1 and S2). (It should be noted that we use the nomenclature of $L_D$ and $L_O$ phases based on our understanding of the system and consistency with prior published works. An alternative interpretation of this system describes it as a single modulated phase or a microemulstion in which the two lipid compositions are denoted as "DSPC/Chol. rich" and "DSPC/Chol. poor".)

**Structural Characterization of Nanodomains.** Small angle neutron scattering (SANS) was used[16] to validate the contrast matching scheme and interrogate the static structure of the system prior to inelastic scattering measurements, which were aimed at measuring the bilayer bending modulus of the nanodomains in situ. SANS is a technique capable of resolving structures with dimensions from ~1 to 100 nm. Scattering data were collected from 60 nm diameter single phase ULVs of $L_O$ ("$L_O$", Figure 1A) and $L_D$ ("$L_D$", Figure 1B) compositions in $D_2O$. We also measured nanodomain containing vesicles in noncontrast enhanced condition (100% $D_2O$), where both phases are "visible" to neutrons ("Domains", Figure 1C). The data are presented in Figure 1F, and are fit by a model using three "slabs" of constant NSLD to model the bilayer:[17] the two slabs correspond to the inner and outer leaflet headgroups, and the other represents the hydrocarbon region, yielding the full bilayer thickness (Table 1, Table S2). The $L_O$ phase was found to be 8.3 ± 0.6 Å thicker than the $L_D$ phase, with the mixed system having an intermediate value reflecting the contributions of both phases to the average acyl chain thickness, in agreement with literature.[7b]

SANS was also measured from nanodomain containing ULVs with specific isotopic substitutions that isolate the scattering from the $L_O$ or $L_D$ regions within the ULVs (compositions in Table S1, "Domains-$L_O$" in 64.5% $D_2O$, Figure 1D, and "Domains-$L_D$" in 93.5% $D_2O$, Figure 1E). Measurements were taken as a function of temperature from 10 to 50 °C, spanning the phase miscibility transition (~40 °C, Figure 2C). Below 40 °C, the $L_D$ phase exhibits excess scattering in the range $0.02 < q < 0.2$ Å$^{-1}$ (Figure 1H) that cannot be adequately described using a slab model. This excess scattering indicates the presence of nanometer scale structures which we analyze using Moore's inversion method[18] to obtain real-space pair distribution functions (PDFs or P(r)) (Figure 1I). These PDFs are then compared directly to models of 60 nm diameter ULVs and 6.8 nm radius discs ("nanodomains") with a thickness of 3.2 nm (Figure 1J). The PDF of the $L_D$ phase in domain containing vesicles at 20 °C (Domains-$L_D$,


DOI: 10.1021/jacs.5b08894
J. Am. Chem. Soc. 2015, 137, 15772−15780

Figure 1I, open red squares) is consistent with the model of nanodomains populating the surface of a sphere, displaying both intra- and interdomain correlations. This result indicates that the $L_D$ phase is discontinuous (i.e., forms nanodomains). Previous experiments on this system[14] had demonstrated only the presence of nanoscopic domains but could not identify which phase comprised the nanodomains.

When the same nanodomain sample was heated above 40 °C (Domains-$L_D$, Figure 1I, solid red squares), the disc-like features disappeared, and the PDF resembled that of a 60 nm diameter ULV. This is due to the breakdown of the contrast matching scheme when the domains and surround become miscible: the lipids in the nanoscopic heterogeneities mix with the continuous phase, forming a single "visible" phase. This observation is consistent with the data from differential scanning calorimetry (DSC) (Figure 2C) and structural measurements (Figures 2B and 3A), showing a broad transition. The hydrocarbon thicknesses of the $L_D$ and $L_O$ phases were obtained by fitting the SANS data ($q > 0.1$ Å$^{-1}$) with a lamellar form factor as a function of temperature from 10 to 50 °C (Figure 3A, Table 1). The bilayer thicknesses of the $L_D$ and $L_O$ regions converge between 30 and 40 °C, consistent with lipid mixing upon domain/surround miscibility. Similarly,

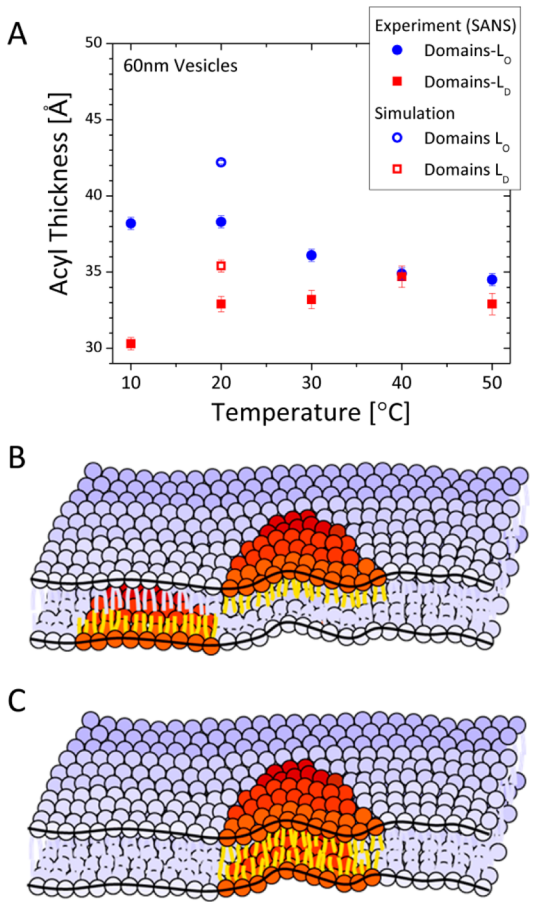


**Figure 3.** Acyl chain thickness is consistent with a bilayer, implying the domains are in-register. (A) the acyl thicknesses from SANS measurements as a function of temperature, including a comparison to the acyl thickness extracted from the atomistic simulations at 20 °C. (B) Unaligned domains would show only a monolayer thickness, whereas aligned domains (C) would show a full bilayer thickness. (error bars are $\pm 2\sigma$).

acyl chain spacings for the pure phases were obtained from separate neutron diffraction[19] measurements (Figure 2C, Figure S1). Little difference was observed in the acyl chain spacing of the $L_D$ phase as a function of temperature (10 to 50 °C). However, $L_O$ acyl chain spacings increased at 40 °C, consistent with increasing chain disorder. This is similar to the temperature where the $L_O$ and $L_D$ regions become miscible.

Returning to the acyl thickness, we note that the observation of a full bilayer thickness (32.9 ± 1.8 Å for the $L_D$ phase and 38.3 ± 2.1 Å for the $L_O$ phase at 20 °C) in samples where one phase has been rendered invisible to neutrons is noteworthy, as it implies that the domains are positionally registered across the bilayer leaflets (Figure 3B,C). In the case of $L_D$ nanodomains, if the domains were antiregistered, the data would have been consistent with the thickness of a monolayer. Similarly, random alignment of domains across bilayer leaflets, would have resulted in only ∼8% of the vesicle area with aligned $L_D$–$L_D$ nanodomains ($L_D$ area fraction is 0.29 in each leaflet). Although positionally registered domains have been observed in phase separated giant unilamellar vesicles,[20] and in recent coarse grained simulations,[21] to our knowledge this is the first experimental verification of positionally registered domains in symmetric ULVs.

**Determination of Nanodomain Bending Modulus.** Having established the ability to isolate the scattering from $L_D$ nanodomains ("Domains-$L_D$"), we used inelastic neutron scattering to investigate their dynamics and mechanical properties. Neutron spin echo spectroscopy (NSE)[22] is a technique sensitive to bilayer motions on time scales of $10^{-10}$–$10^{-7}$s, and over length scales of ∼0.1–100 nm. It is therefore an ideal tool to probe the bilayer's undulational motions, which are characteristic of bending rigidity.[23] We performed NSE measurements[24] on four samples at 20 °C: $L_O$ only vesicles in $D_2O$ (Figure 1A), $L_D$ only vesicles in $D_2O$ (Figure 1B), coexisting $L_O/L_D$ vesicles with no contrast enhancement (Domains) in $D_2O$ (Figure 1C), and $L_D$ nanodomains ("Domains-$L_{D''}$") in 93.5% $D_2O/H_2O$ (Figure 1E). The $L_D$ nanodomain measurements (Figure 3D) focused on a single $q$ value of 0.055 Å$^{-1}$. This was dictated by the fact that the "Domains-$L_D$" sample's scattering is ∼30 times weaker than the other samples, in addition to possessing a higher intrinsic incoherent scattering background (Due to the unavailability of select deuterated lipids, the "Domains-$L_O$" sample was not measured with NSE. Further details on this point can found in the SI).

NSE measurements report the intermediate scattering function (ISF), or $S(q,\tau)/S(q,0)$. This can be thought of as the probability of finding atomic pair correlations at a distance, $2\pi/q$, after a time, $\tau$ (Figure 4A–D). In order to relate the undulational dynamics to the bilayer bending modulus, we have adopted the model of Zilman and Granek.[23] This model treats the bilayer as a flat sheet, a condition considered valid for systems with $qR \gg 1$. In this study $qR$ was between 15 and 33, where $R$ = 300 Å and the $q$-range was 0.05–0.11 Å$^{-1}$. In this case the ISF for undulations then decays as

$$\frac{S(q,\tau)}{S(q,0)} = Ae^{-(\Gamma(q)\tau)^{2/3}}, \quad (1)$$

where $A$ is a normalization constant (typically set to 1). The relaxation rate, $\Gamma(q)$, is a function of the scattering wave vector, $q$, and is related to the bilayer bending modulus $\kappa$ through the relation[25]


DOI: 10.1021/jacs.5b08894
J. Am. Chem. Soc. 2015, 137, 15772–15780

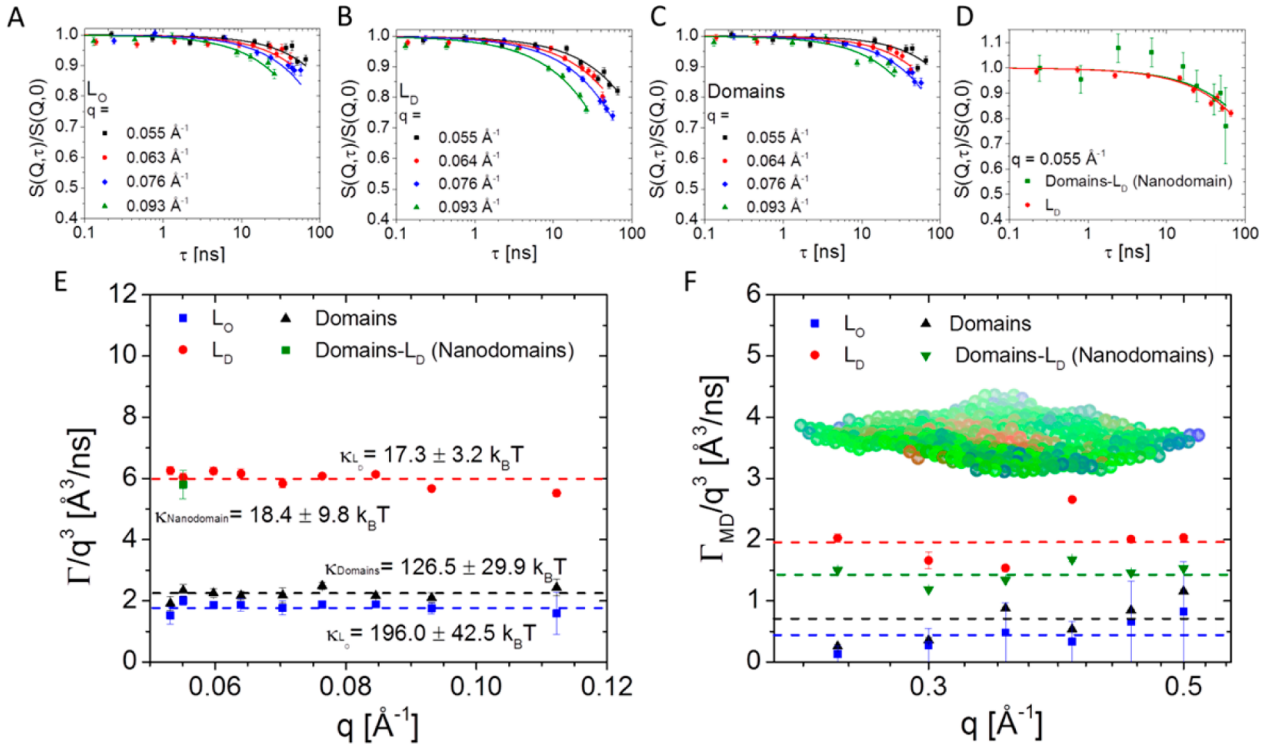


**Figure 4.** Representative ISFs from NSE experiments with fits to the data using the Zillman-Granek model (A–D) (error bars are $\pm 2\sigma$).[23] (E) Undulational relaxation times obtained from the fit to the data follows the predicted $q^{-3}$ dependence, revealing a dynamical decoupling between the $L_D$ nanodomain and its surround. (F) Undulatory relaxation times calculated from all-atom MD simulations, revealing a trend in the dynamics that is qualitatively consistent with experimental observation, including the dynamical decoupling of the nanodomains from the surrounding phase (error bars represent $\pm 2\sigma$ of the fit). Inset shows an MD snapshot of a patch rendered with a grid of pseudoatoms at the local center of mass.

$$\Gamma(q) = 0.0058\left(\frac{k_B T}{\kappa}\right)^{1/2}\frac{k_B T}{\eta}q^3. \quad (2)$$

Here, $\eta$, is the solvent viscosity, $k_B$ is Boltzmann's constant, and $T$ is the temperature. It is convenient to plot the data as $\Gamma(q)/q^3$ versus $q$, due to the predicted $q^3$ dependence (Figure 4E). The data is expected to exhibit a constant value in this presentation that is inversely proportional to the square root of the bending modulus.

The data do in fact show a $q^{-3}$ dependence in the dynamics. We then calculate the bending moduli from the data, showing that the $L_O$ sample is more rigid than the $L_D$ sample ($\kappa_{LD} = 17.3 \pm 3.2\ k_BT$, $\kappa_{LO} = 196.0 \pm 42.5\ k_BT$), as one might expect. The modulus of the POPC rich $L_D$ phase is similar to what has been reported for fluid POPC/Chol. bilayers at 22 °C.[26] However, the modulus for the DSPC rich $L_O$ phase is more than two times softer than a DSPC gel phase bilayer at 45 °C,[25b] and in good agreement with $L_O$ phases from lipid mixtures such as sphingomyelin/Chol. (198 $k_BT$)[27] or sphingomyelin/DOPC/Chol. (168 $k_BT$).[28] Interestingly, the modulus of the nanodomains ("Domains-$L_D$", $\kappa_{Nanodomain} = 18.4 \pm 9.8\ k_BT$) is indistinguishable from the pure (single phase) $L_D$ sample. In contrast to this, the bending modulus of the noncontrast matched domains sample ("Domains") has an intermediate rigidity ($\kappa_{Domains} = 126.5 \pm 29.9\ k_BT$), reflecting the ensemble nature of the measurement. This shows that mechanical properties connected to the local composition persist even at the nanometer length scale.

Further evidence of domain registration is also seen through the intermediate rigidity of the noncontrast matched system ("Domains"). This intermediate rigidity reflects the ensemble nature of that measurement, as both the $L_D$ and $L_O$ phases contribute to the scattering. The nanodomains sample ("Domains-$L_D$"), on the other hand, is only sensitive to the motions from the $L_D$ nanodomains (the $L_O$ surround is "invisible" to neutrons), but is otherwise structurally identical to the "Domains" sample, providing an important control. Randomly aligned or antiregistered domains in the inner and outer bilayer leaflets would have resulted in a larger bending modulus than the $L_D$ sample because the nanodomains would have been across from an $L_O$ portion of the bilayer (Figure 3B). Thus, the similar bending moduli of the $L_D$-nanodomains and the bulk $L_D$ composition is further evidence of domain registry across the bilayer leaflets.

The primary significance of this result relates to domain formation. Although different bending moduli for coexisting phases have been previously reported in macroscopically phase separated bilayers,[29] our observations show that even for nanoscopic domains on the length scale of lipid rafts, differences in the bending moduli of the two lipid regions persist. Moreover, these differences are capable of contributing to the free energy of the system[30] and influencing phase behavior.[8,9i,m]

**MD Simulation: Molecular Details of the Domain Interface.** All-atom MD simulations were performed to compare with our structural and bending modulus data, as well as to provide a more detailed description of the nanodomain interface. The simulated lipid systems were symmetric planar bilayer patches in explicit water. They were compositionally similar to those studied experimentally, namely: $L_O$, $L_D$, and $L_D$ nanodomains coexisting in an $L_O$ bilayer (Table S1). The $L_O$ and $L_D$ models were 12 nm × 12


DOI: 10.1021/jacs.5b08894
J. Am. Chem. Soc. 2015, 137, 15772–15780

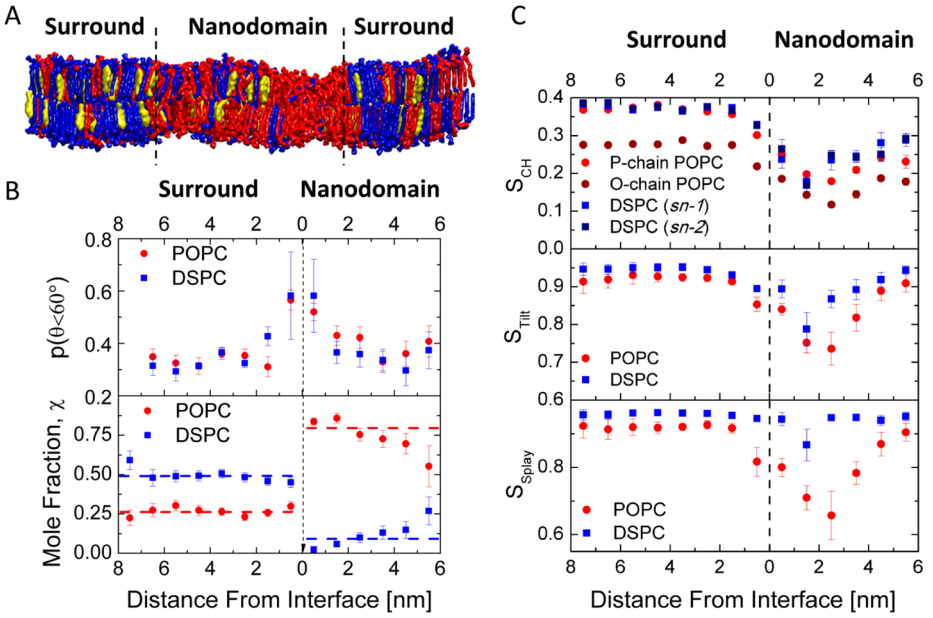


**Figure 5.** Molecular dynamics simulations reveal details of the domain interface. (A) Cross-section of the simulated patch containing an $L_D$ nanodomain surrounded by the $L_O$ phase after 150 ns of simulation (DSPC, blue; POPC, red; and cholesterol, yellow). (B) Lipid composition and orientation as a function of distance from the domain interface. Preferential alignment of the *sn-2* chains of both DSPC and POPC toward the phase boundary. $\theta$ reflects the rotational alignment of the *sn-2* chain toward the domain interface. $p(\theta < 60°)$ is the probability that the angle $\theta$ is less than 60°: random alignment would have a value near 0.33. An enrichment of POPC is evident near the interface in the bottom panel (dotted lines represent the average composition). (C) Order parameters as a function of distance from an arbitrary nanodomain-surround interface. $S_{CH}$, reflects the angle between the CH bond and the bilayer normal, similar to what is observed by NMR. $S_{Tilt}$ is based on the average tilt angle of a lipid relative to the bilayer normal, and $S_{Splay}$ reflects the divergence of local lipid tilt. Disorder associated with the interfacial region is indicated from the OPs, with a minimum observed ∼1−2 nm from the interface. (error bars represent $\pm 2\sigma$).

nm patches assembled using the PACKMOL package.[31] In order to study nanodomain properties, we preassembled an in-register, 6.8 nm radius $L_D$ domain surrounded by an $L_O$ phase (24 nm × 24 nm). Further details are found in the SI.

The structural parameters from the simulated lipid patches are summarized in Table 1 and Figure 3A, and are in good agreement with those from experiment. We also find qualitative agreement between the bilayer unduational dynamics (ISFs) from simulation[32] and experiment. However, limitations imposed by the simulation box size and the duration of the simulation, the long wavelength undulation modes observed experimentally are not captured by simulation. In other words, we cannot reliably determine the bending modulus from the undulation dynamics calculated from the MD trajectories. Knowing this, we can only qualitatively compare the undulational dynamics after correcting for thickness fluctuations.[25b] This comparison shows that the pure $L_O$ patch is less dynamic than the pure $L_D$ patch, and the nanodomain region is more dynamic than the average of the full domain containing patch. Both findings are consistent with the results of our neutron scattering experiments.

An alternative method of computing the bending modulus from MD trajectories has been proposed by Khelashvili et al.,[33] which considers the splay and tilt angles of lipid molecules (Figure 5). This analysis show a similar trend, with the $L_D$ nanodomain having a lower bending modulus than the $L_O$ surround, and the full $L_O$ patch was stiffer than the $L_D$ patch, again consistent with the observed and calculated undulational dynamics (Table 1).

The simulations also allow us to interrogate the nanodomain system at a molecular level, particularly the interfacial region where a visual inspection of the bilayer cross-section (Figure 4A) reveals bilayer thinning and acyl chain disorder. This provides us with some insight as to why the dynamics of the nanodomains are not somewhat slower than those of "pure" $L_D$ vesicles. One might expect that undulational modes with wavelengths larger than the domain size would reflect the rigidity of both phases. This is, however, not what we observe. The presence of a flexible region between the $L_D$ nanodomain and the $L_O$ surround seemingly allows a degree of autonomous motion of the $L_D$ nanodomains on short length scales, a notion that is more in line with our experimental results.

Computing the molecular composition, orientation, and order parameters (OPs) from the simulations allows us to explore the interface more quantitatively. In Figure 5 the parameters determined from the simulations are presented as a function of distance from the $L_O$−$L_D$ interface, their respective definitions are discussed in detail in the SI and Figures S3, S4, S5, and S6. Figure 5C shows clear local minima in the OPs near the interface. These are understood to be a compensatory overshoot in the order parameters,[34] similar to what is predicted by theories of curvature[9a−c,35] or line-active molecule[9f,h,j−l] stabilized interfaces. It is also known that lipid splay and tilt are intimately connected with local rigidity in the bilayer.[33,34,36] These minima in $S_{Tilt}$ and $S_{Splay}$, along with the thinning of the bilayer, imply local flexibility at the interface.

It is also interesting to note that the simulations reveal a small increase in POPC concentration at the nanodomain interface, in addition to preferential orientation (Figure 5B). DSPC is also found to preferentially orient at the interface. Taken together, these phenomena imply a reduction in the translational and rotational entropy as a result of the accumulated molecules at the interface.[9f] The alignment appears to orient the *sn-2* chain (and the headgroup in the


DOI: 10.1021/jacs.5b08894
J. Am. Chem. Soc. 2015, 137, 15772−15780

*sn-3* position) toward the interface for both lipids (POPC and DSPC), and from both sides (nanodomain and surround), consistent with tilted lipids near the thinned region of the bilayer.

These observations are interesting in the context of models for domain formation based on line activity. In particular, mixed acyl lipids (such as POPC) have been suggested as line active molecules,[9f,37] where the lipid preferentially orients at an interface, straddling the two phases. In the case of POPC, the saturated chain (*sn-1* palmitoyl in this case) is hypothesized to associate with the $L_O$ phase, with the unsaturated chain (*sn-2* oleoyl in this case) preferring the $L_D$ phase.[9f] In this way, the acyl chains can pack more favorably, reducing the interfacial energy and stabilizing the domain interface. In general, the favorable packing associated with orientational ordering contributes significantly to the free energy, as seen in lipid melting transitions.[38] Moreover, preferential lipid orientation near the interface can be thought to stabilize the system, favoring an increase in interfacial length, while maintaining the total areas of the two phases. Theoretically, this can act in combination with other parameters controlling the free energy of the system, effectively reducing domain size and maximizing the ratio of interface to total domain area. Enrichment of POPC near the interface is consistent with aspects of these line activity based mechanisms. However, we also observe that both POPC and DSPC show a preferential orientation with respect to the interface. This implies that it is not exclusively the mixed acyl chain nature of POPC that is driving orientation and interfacial stabilization. The effect could be a more generic consideration of the *sn-2* chain (and headgroup in the *sn-3* position) as they relate to accommodating the difference in bilayer thickness[7b] and spontaneous curvature[9a,c,39] between the two "phases". This is consistent with recent experimental observations that straight chain and mixed acyl lipids have similar effects on domain size.[40]

Lipid domains and the surrounding phase likely differ in several properties such as their bending modulus, shown in this work, and their spontaneous curvature. We are able to calculate the spontaneous curvatures of the $L_O$ and $L_D$ regions ($-0.097$ $nm^{-1}$ and $-0.068$ $nm^{-1}$, respectively)[7b] suggesting that there is a difference in spontaneous curvature. Local curvature influences lipid packing, as measured by their tilt, splay, and orientation,[34] results consistent with our MD simulations. Theoretical work[9c,i,39] does suggest that local curvature can also play an important role in lipid phase behavior. In some ways this is similar to differences in bending moduli between the two phases, as both spontaneous curvature and the bending modulus contribute to the free energy of the system.[30]

## CONCLUSIONS

Using a novel contrast matching strategy and inelastic neutron scattering we have shown that in-register, ∼ 13 nm diameter lipid domains in 60 nm diameter ULV's possess a different bending modulus than the surrounding continuous bilayer. This result is significant in the context of understanding what physical mechanisms underlay the formation of nanoscopic lipid heterogeneities and potentially, lipid rafts. Differences in bending moduli of the two "phases" contribute to the system's free energy, potentially stabilizing domain size by competing with interfacial energy.[8,9i,m] This is similar to, and perhaps in connection with, the way that differences in the spontaneous curvature[9a−c,i,35,39] are thought to stabilize domains. Here we have demonstrated this difference in bending modulus in a model bilayer containing nanoscopic heterogeneities similar in size to lipid rafts. Our analysis also provides experimental support to those who have suggested that curvature and interfacial effects should be considered in new models of lipid phase behavior.

Neutron scattering, in combination with NSLD contrast matching techniques, is uniquely capable of providing experimental measurements of the structure and dynamics of the nanoscopic structures, such as the lipid heterogeneities central to the lipid raft hypothesis. In this study, we were able to determine the in situ mechanical properties of lipid nanodomains, a measurement that cannot be obtained by other experimental techniques. Furthermore, this approach of isolating the structure and dynamics of a coexisting phase using NSLD contrast matching can be extended to other hydrogen rich, phase-separated systems, including lipid bilayer systems containing membrane proteins or candidate drug molecules. MD simulations are a natural complement to neutron scattering studies, providing information on time and length scales similar to neutron scattering, in addition to molecular details that are not experimentally accessible. Here, atomistic MD has shown us the organization of lipids at the domain interface, and placed our results in the context of existing models of domain formation.

The preservation of bulk phase properties (composition, thickness, and bending modulus) within nanoscopic domains is consistent with their hypothesized role as scalable compartments in biological membranes, providing consistent physical environments to resident membrane proteins. It will be interesting to extend our experimental and simulation approach to other domain-containing lipid compositions of different domain sizes in order to understand if our experimental results are typical of lipid behavior, or a special case for nanoscopic domains. In conclusion, it seems appropriate that in addition to local differences in the bending modulus, we find indications of multiple mechanisms that can contribute to stabilizing nanoscopic lipid heterogeneities. The complexity and compositional diversity of natural biological membranes makes it likely that multiple mechanisms are exploited by living systems to regulate the structure and functions of lipid rafts and their resident membrane proteins in vivo.

## ASSOCIATED CONTENT

### Supporting Information

The Supporting Information is available free of charge on the ACS Publications website at DOI: 10.1021/jacs.5b08894.

Detailed method section, 6 additional data figures, 2 additional tables, and associated discussion[41−54]. (PDF)

## AUTHOR INFORMATION


### Corresponding Authors

*nickelsjd@ornl.gov

*katsarasj@ornl.gov


### Notes

The authors declare no competing financial interest.

## ACKNOWLEDGMENTS

The authors gratefully acknowledge Professors F. Brown, R. Epand, G.W. Feigenson, and M. Schick for a critical reading of the manuscript and insightful conversations; J. Neuefeind, C. Gao, R. Moody, M. Doktorova, M. Cochran, and P. Zolnierczuk for technical assistance; and Prof. H. Riezman



DOI: 10.1021/jacs.5b08894
J. Am. Chem. Soc. 2015, 137, 15772−15780

(Univ. of Geneva) for the generous gift of cholesterol-producing yeast strain and protocol. JDN is partially supported by the U.S. DOE BES through the EPSCoR Grant No. DE-FG02-08ER46528. JK is supported through the Scientific User Facilities Division of the DOE Office of Basic Energy Sciences (BES), under contract no. DE-AC05 00OR2275. XC is partially supported by the Laboratory Directed R&D (LDRD) fund P7394 at the Oak Ridge National Laboratory. This research used resources of the Oak Ridge Leadership Computing Facility at the Oak Ridge National Laboratory, which is supported by the Office of Science of the U.S. Department of Energy under Contract No. DE-AC05-00OR22725. Research conducted at ORNL's Spallation Neutron Source was sponsored by the Scientific User Facilities Division, Office of Basic Energy Sciences, US Department of Energy. Oak Ridge National Laboratory is managed by UT-Battelle, LLC under US DOE Contract No. DE-AC05-00OR22725.

## REFERENCES

(1) (a) Simons, K.; Van Meer, G. *Biochemistry* **1988**, *27*, 6197−6202. (b) Klausner, R.; Kleinfeld, A.; Hoover, R.; Karnovsky, M. J. *J. Biol. Chem.* **1980**, *255*, 1286−1295. (c) Brown, D. A.; Rose, J. K. *Cell* **1992**, *68*, 533−544. (d) Song, K. S.; Li, S.; Okamoto, T.; Quilliam, L. A.; Sargiacomo, M.; Lisanti, M. P. *J. Biol. Chem.* **1996**, *271*, 9690−9697. (e) Jacobson, K.; Mouritsen, O. G.; Anderson, R. G. *Nat. Cell Biol.* **2007**, *9*, 7−14. (f) Simons, K.; Ikonen, E. *Nature* **1997**, *387* (6633), 569−572. (g) Nickels, J. D.; Smith, J. C.; Cheng, X. *Chem. Phys. Lipids* **2015**, DOI: 10.1016/j.chemphyslip.2015.07.012.

(2) Lingwood, D.; Simons, K. *Science* **2010**, *327*, 46−50.

(3) Simons, K.; Toomre, D. *Nat. Rev. Mol. Cell Biol.* **2000**, *1*, 31−39.

(4) (a) Simons, K.; Ehehalt, R. *J. Clin. Invest.* **2002**, *110*, 597−603. (b) Nguyen, D. H.; Hildreth, J. E. *J. Virol.* **2000**, *74*, 3264−3272. (c) Abrami, L.; van der Goot, F. G. *J. Cell Biol.* **1999**, *147*, 175−184. (d) Dick, R. A.; Goh, S. L.; Feigenson, G. W.; Vogt, V. M. *Proc. Natl. Acad. Sci. U. S. A.* **2012**, *109*, 18761−18766.

(5) Yethiraj, A.; Weisshaar, J. C. *Biophys. J.* **2007**, *93*, 3113−3119.

(6) Turner, M. S.; Sens, P.; Socci, N. D. *Phys. Rev. Lett.* **2005**, *95*, 168301.

(7) (a) Feigenson, G. W. *Biochim. Biophys. Acta, Biomembr.* **2009**, *1788*, 47−52. (b) Heberle, F. A.; Petruzielo, R. S.; Pan, J.; Drazba, P.; Kučerka, N.; Standaert, R. F.; Feigenson, G. W.; Katsaras, J. *J. Am. Chem. Soc.* **2013**, *135*, 6853−9. (c) Simons, K.; Vaz, W. L. C. *Annu. Rev. Biophys. Biomol. Struct.* **2004**, *33*, 269−295. (d) Armstrong, C. L.; Marquardt, D.; Dies, H.; Kučerka, N.; Yamani, Z.; Harroun, T. A.; Katsaras, J.; Shi, A.-C.; Rheinstädter, M. C. *PLoS One* **2013**, *8*, e66162. (e) Connell, S. D.; Heath, G.; Olmsted, P. D.; Kisil, A. *Faraday Discuss.* **2013**, *161*, 91−111. (f) Toppozini, L.; Meinhardt, S.; Armstrong, C. L.; Yamani, Z.; Kučerka, N.; Schmid, F.; Rheinstädter, M. C. *Phys. Rev. Lett.* **2014**, *113*, 228101.

(8) Seul, M.; Andelman, D. *Science* **1995**, *267*, 476−483.

(9) (a) Schick, M. *Phys. Rev. E* **2012**, *85*, 031902. (b) Shlomovitz, R.; Maibaum, L.; Schick, M. *Biophys. J.* **2014**, *106*, 1979−1985. (c) Meinhardt, S.; Vink, R. L.; Schmid, F. *Proc. Natl. Acad. Sci. U. S. A.* **2013**, *110*, 4476−4481. (d) Veatch, S. L.; Soubias, O.; Keller, S. L.; Gawrisch, K. *Proc. Natl. Acad. Sci. U. S. A.* **2007**, *104*, 17650−17655. (e) Honerkamp-Smith, A. R.; Cicuta, P.; Collins, M. D.; Veatch, S. L.; den Nijs, M.; Schick, M.; Keller, S. L. *Biophys. J.* **2008**, *95*, 236−246. (f) Brewster, R.; Pincus, P.; Safran, S. *Biophys. J.* **2009**, *97*, 1087−1094. (g) Hancock, J. F. *Nat. Rev. Mol. Cell Biol.* **2006**, *7*, 456−462. (h) Palmieri, B.; Grant, M.; Safran, S. A. *Langmuir* **2014**, *30*, 11734−11745. (i) Amazon, J. J.; Goh, S. L.; Feigenson, G. W. *Phys. Rev. E* **2013**, *87*, 022708. (j) Hirose, Y.; Komura, S.; Andelman, D. *Phys. Rev. E* **2012**, *86*, 021916. (k) Yamamoto, T.; Brewster, R.; Safran, S. *Europhys. Lett.* **2010**, *91*, 28002. (l) Yamamoto, T.; Safran, S. A. *Soft Matter* **2011**, *7*, 7021−7033. (m) Leibler, S.; Andelman, D. *J. Phys.* **1987**, *48*, 2013−2018.

(10) Arriaga, L.; Rodriguez-Garcia, R.; López-Montero, I.; Farago, B.; Hellweg, T.; Monroy, F. *Eur. Phys. J. E: Soft Matter Biol. Phys.* **2010**, *31*, 105−113.

(11) (a) de Almeida, R. F.; Fedorov, A.; Prieto, M. *Biophys. J.* **2003**, *85*, 2406−2416. (b) Hammond, A.; Heberle, F.; Baumgart, T.; Holowka, D.; Baird, B.; Feigenson, G. *Proc. Natl. Acad. Sci. U. S. A.* **2005**, *102*, 6320−6325.

(12) Konyakhina, T. M.; Goh, S. L.; Amazon, J.; Heberle, F. A.; Wu, J.; Feigenson, G. W. *Biophys. J.* **2011**, *101*, 8−10.

(13) (a) Dietrich, C.; Bagatolli, L.; Volovyk, Z.; Thompson, N.; Levi, M.; Jacobson, K.; Gratton, E. *Biophys. J.* **2001**, *80*, 1417−1428. (b) Samsonov, A. V.; Mihalyov, I.; Cohen, F. S. *Biophys. J.* **2001**, *81*, 1486−1500. (c) Veatch, S. L.; Keller, S. L. *Biochim. Biophys. Acta, Mol. Cell Res.* **2005**, *1746*, 172−185.

(14) Heberle, F. A.; Wu, J.; Goh, S. L.; Petruzielo, R. S.; Feigenson, G. W. *Biophys. J.* **2010**, *99*, 3309−3318.

(15) Zhao, J.; Wu, J.; Heberle, F. A.; Mills, T. T.; Klawitter, P.; Huang, G.; Costanza, G.; Feigenson, G. W. *Biochim. Biophys. Acta, Biomembr.* **2007**, *1768*, 2764−2776.

(16) Zhao, J. K.; Gao, C. Y.; Liu, D. *J. Appl. Crystallogr.* **2010**, *43*, 1068−1077.

(17) (a) King, G. I.; White, S. H. *Biophys. J.* **1986**, *49*, 1047−1054. (b) White, S. H.; King, G. I. *Proc. Natl. Acad. Sci. U. S. A.* **1985**, *82*, 6532−6536.

(18) Moore, P. B. *J. Appl. Crystallogr.* **1980**, *13*, 168−175.

(19) Neuefeind, J.; Feygenson, M.; Carruth, J.; Hoffmann, R.; Chipley, K. K. *Nucl. Instrum. Methods Phys. Res., Sect. B* **2012**, *287*, 68−75.

(20) Korlach, J.; Schwille, P.; Webb, W. W.; Feigenson, G. W. *Proc. Natl. Acad. Sci. U. S. A.* **1999**, *96*, 8461−8466.

(21) Ackerman, D.; Feigenson, G. W. *J. Phys. Chem. B* **2015**, *119*, 4240−4250.

(22) Mezei, F. *Eur. Phys. J. A* **1972**, *255*, 146−160.

(23) Zilman, A.; Granek, R. *Phys. Rev. Lett.* **1996**, *77*, 4788.

(24) Ohl, M.; Monkenbusch, M.; Arend, N.; Kozielewski, T.; Vehres, G.; Tiemann, C.; Butzek, M.; Soltner, H.; Giesen, U.; Achten, R.; Stelzer, H.; Lindenau, B.; Budwig, A.; Kleines, H.; Drochner, M.; Kaemmerling, P.; Wagener, M.; Möller, R.; Iverson, E. B.; Sharp, M.; Richter, D. *Nucl. Instrum. Methods Phys. Res., Sect. A* **2012**, *696*, 85−99.

(25) (a) Lee, J.-H.; Choi, S.-M.; Doe, C.; Faraone, A.; Pincus, P. A.; Kline, S. R. *Phys. Rev. Lett.* **2010**, *105*, 038101. (b) Woodka, A. C.; Butler, P. D.; Porcar, L.; Farago, B.; Nagao, M. *Phys. Rev. Lett.* **2012**, *109*, 058102. (c) Watson, M. C.; Brown, F. L. *Biophys. J.* **2010**, *98*, L9−L11.

(26) Arriaga, L. R.; López-Montero, I.; Monroy, F.; Orts-Gil, G.; Farago, B.; Hellweg, T. *Biophys. J.* **2009**, *96*, 3629−3637.

(27) Gracià, R. S.; Bezlyepkina, N.; Knorr, R. L.; Lipowsky, R.; Dimova, R. *Soft Matter* **2010**, *6*, 1472−1482.

(28) Semrau, S.; Idema, T.; Holtzer, L.; Schmidt, T.; Storm, C. *Phys. Rev. Lett.* **2008**, *100*, 088101.

(29) (a) Baumgart, T.; Das, S.; Webb, W.; Jenkins, J. *Biophys. J.* **2005**, *89*, 1067−1080. (b) Baumgart, T.; Hess, S. T.; Webb, W. W. *Nature* **2003**, *425*, 821−824.

(30) Helfrich, W. *Z. Naturforsch. C* **1973**, *28*, 693−703.

(31) Martínez, L.; Andrade, R.; Birgin, E. G.; Martínez, J. M. *J. Comput. Chem.* **2009**, *30*, 2157−2164.

(32) Lindner, B.; Smith, J. C. *Comput. Phys. Commun.* **2012**, *183*, 1491−1501.

(33) Khelashvili, G.; Kollmitzer, B.; Heftberger, P.; Pabst, G.; Harries, D. *J. Chem. Theory Comput.* **2013**, *9*, 3866−3871.

(34) Kuzmin, P. I.; Akimov, S. A.; Chizmadzhev, Y. A.; Zimmerberg, J.; Cohen, F. S. *Biophys. J.* **2005**, *88*, 1120−1133.

(35) Gompper, G.; Schick, M. *Phys. Rev. Lett.* **1990**, *65*, 1116.

(36) Watson, M. C.; Brandt, E. G.; Welch, P. M.; Brown, F. L. *Phys. Rev. Lett.* **2012**, *109*, 028102.

(37) Palmieri, B.; Safran, S. A. *Langmuir* **2013**, *29*, 5246−5261.

(38) Tristram-Nagle, S.; Nagle, J. F. *Chem. Phys. Lipids* **2004**, *127*, 3−14.



DOI: 10.1021/jacs.5b08894
*J. Am. Chem. Soc.* 2015, 137, 15772−15780

(39) (a) Kawakatsu, T.; Andelman, D.; Kawasaki, K.; Taniguchi, T. *J. Phys. II* **1993**, *3*, 971−997. (b) Taniguchi, T.; Kawasaki, K.; Andelman, D.; Kawakatsu, T. *J. Phys. II* **1994**, *4*, 1333−1362.
(40) Heberle, F. A.; Doktorova, M.; Goh, S. L.; Standaert, R. F.; Katsaras, J.; Feigenson, G. W. *J. Am. Chem. Soc.* **2013**, *135*, 14932−14935.
(41) Souza, C. M.; Schwabe, T. M.; Pichler, H.; Ploier, B.; Leitner, E.; Guan, X. L.; Wenk, M. R.; Riezman, I.; Riezman, H. *Metab. Eng.* **2011**, *13*, 555−569.
(42) Breivik, O.; Owades, J. *J. Agric. Food Chem.* **1957**, *5*, 360−363.
(43) (a) Greenwood, A. I.; Tristram-Nagle, S.; Nagle, J. F. *Chem. Phys. Lipids* **2006**, *143*, 1−10. (b) Kučerka, N.; Nieh, M.-P.; Katsaras, J. *Biochim. Biophys. Acta, Biomembr.* **2011**, *1808*, 2761−2771. (c) Tristram-Nagle, S.; Liu, Y.; Legleiter, J.; Nagle, J. F. *Biophys. J.* **2002**, *83*, 3324−3335. (d) Tristram-Nagle, S.; Petrache, H. I.; Nagle, J. F. *Biophys. J.* **1998**, *75*, 917−925.
(44) Sears, V. F. *Neutron News* **1992**, *3*, 26−37.
(45) Büldt, G.; Gally, H.; Seelig, A.; Seelig, J.; Zaccai, G. *Nature* **1978**, *271*, 182−184.
(46) Nagle, J. F.; Zhang, R.; Tristram-Nagle, S.; Sun, W.; Petrache, H. I.; Suter, R. M. *Biophys. J.* **1996**, *70*, 1419−1431.
(47) Nickels, J. D.; O'Neill, H.; Hong, L.; Tyagi, M.; Ehlers, G.; Weiss, K. L.; Zhang, Q.; Yi, Z.; Mamontov, E.; Smith, J. C.; Sokolov, A. P. *Biophys. J.* **2012**, *103*, 1566−75.
(48) (a) Feller, S. E.; Zhang, Y.; Pastor, R. W.; Brooks, B. R. *J. Chem. Phys.* **1995**, *103*, 4613−4621. (b) Martyna, G. J.; Tobias, D. J.; Klein, M. L. *J. Chem. Phys.* **1994**, *101*, 4177−4189.
(49) (a) Darden, T.; York, D.; Pedersen, L. *J. Chem. Phys.* **1993**, *98*, 10089−10092. (b) Essmann, U.; Perera, L.; Berkowitz, M. L.; Darden, T.; Lee, H.; Pedersen, L. G. *J. Chem. Phys.* **1995**, *103*, 8577−8593.
(50) Tuckerman, M.; Berne, B. J.; Martyna, G. J. *J. Chem. Phys.* **1992**, *97*, 1990−2001.
(51) Ryckaert, J.-P.; Ciccotti, G.; Berendsen, H. J. *J. Comput. Phys.* **1977**, *23*, 327−341.
(52) Phillips, J. C.; Braun, R.; Wang, W.; Gumbart, J.; Tajkhorshid, E.; Villa, E.; Chipot, C.; Skeel, R. D.; Kale, L.; Schulten, K. *J. Comput. Chem.* **2005**, *26*, 1781−1802.
(53) (a) Feller, S. E.; Yin, D.; Pastor, R. W.; MacKerell, A. D., Jr *Biophys. J.* **1997**, *73*, 2269. (b) Klauda, J. B.; Venable, R. M.; Freites, J. A.; O'Connor, J. W.; Tobias, D. J.; Mondragon-Ramirez, C.; Vorobyov, I.; MacKerell, A. D., Jr; Pastor, R. W. *J. Phys. Chem. B* **2010**, *114*, 7830−7843.
(54) Levine, Z. A.; Venable, R. M.; Watson, M. C.; Lerner, M. G.; Shea, J.-E.; Pastor, R. W.; Brown, F. L. *J. Am. Chem. Soc.* **2014**, *136*, 13582−13585.


DOI: 10.1021/jacs.5b08894
*J. Am. Chem. Soc.* 2015, 137, 15772−15780